

# Microstructural and Thermal Properties of Porous Aluminum Filled with Nanocrystalline Silicon

Taher Ghrib\*

Laboratory of Physical Alloys (LPA), Faculty of Science of Dammam, University of Dammam, Saudi Arabia, [taher.ghrib@yahoo.fr](mailto:taher.ghrib@yahoo.fr).

Amal Lafy Al-Otaibi

Laboratory of Physical Alloys (LPA), Faculty of Science of Dammam, University of Dammam, Saudi Arabia, [amalotaibi@uod.edu.sa](mailto:amalotaibi@uod.edu.sa).

Munirah Abdullah Almessiere

Laboratory of Physical Alloys (LPA), Faculty of Science of Dammam, University of Dammam, Saudi Arabia, [malmessiere@uod.edu.sa](mailto:malmessiere@uod.edu.sa).

## Abstract

In this work, the structural, thermal and optical properties of porous aluminum thin film carried out with various intensities of the anodization current in sulfuric acid. The obtained pores at the surface are filled by nanocrystalline silicon (nc-Si) thin films deposited by plasma enhancement chemical vapor deposition (PECVD), which the role is to improving its optical absorption and thermal properties. The prepared sample is an assembly of three different media such as Al sample/ Porous aluminum layer filled with silicon (PAS)/ nanocrystallite silicon layer (nc-Si). The effect of anodization current on the microstructure of porous aluminium and the effect of the deposited silicon layer were systematically studied by atomic force microscopy (AFM), X-ray diffraction (XRD) and Raman spectroscopy. The thermal properties such as the thermal conductivity (K) and thermal diffusivity (D) were determined by the photo-thermal deflection (PTD) technique, which is a non-destructive technique. Based on this full characterization, it is demonstrated that the thermal and optical characteristics of this films are directly correlated to their micro-structural properties.

Keywords: Porous Aluminum; thermal conductivity; thermal diffusivity; gap energy  
Article history: Received December 31, 2013; Accepted February 4, 2014

## 1. Introduction

In view of their practical importance, aluminum porous materials were intensively studied in the last decade with various analytical techniques (see references from 2002 by Nielsch et al., to 2012 by Liu et al.). There was considerable interest primarily for the reason of its self organized pores that have quasi-cylindrical shape and well aligned and the pores sizes which are in the vicinity of nanometers range constitute a technological revolution and find now many applications such as filtration membranes such that realized by Sulka et al., 2011 or by Barbosa et al., 2012, as backing for manufacturing nanowires used by Wang et al., 2011 or Huang et al., 2012 and

as photonic crystals (see for example the work of Hu et al., 2009), as humidity sensors according to Kurbanov et al., 2007 or Juhász et al., 2009 and Kashi et al., 2012 or as cathodes for organic light emitting diodes as those of Wang et al., 2007 and Kim et al., 2008. The scientists have been focused on the fabrication of organized nano-pores by electrochemical methods by simple variation of the anodization parameters, such as voltage and electrolyte solution composition. In the literature many attempts are reported in order to find relationships between porosity, thermal properties studied by Zhuo et al., 2011 and Dyga et al., 2012, optical properties studied by Stojadinovic et al., 2009, and this by exploring the effect of size, form and

\* Corresponding author

density of the pores. For photovoltaic applications knowing sample emissivity, absorption and thermal properties is a primordial issue for solar energy development. It was reported also that nc-Si thin films elaborated by PECVD on a porous aluminum structure leads to the synthesis of material of great electronic quality. Thus cells based on crystalline silicon on porous aluminum offer an exciting possibility of constructing and fabricating compact photovoltaic and thermal solar collectors by direct cell deposition on a suitable porous aluminum. The fine tuning of microstructure and of the thermal properties of the elaborated films is a primordial step for controlling the functionality of the desired device. The current anodization parameter has directly an impact to the surface roughness and film density, which in turn influence the physical properties such as thermal and optical properties. The thermal properties of the deposited films are examined by photothermal deflection (PTD) technique in 1994 by Bertolotti et al., and by Ghrib et al. who have correlated them to the film microstructure. In this context, we have tailored to study the anodization current effect in the microstructure of the porous aluminium (PA) layer and the effect of the deposition of silicon layer on its optical and thermal properties.

## 2. Experiments processing

High-purity aluminum foil (99.997%), 0.25 mm thick was used as a starting material. Before anodizing the aluminum paper was rinsed in a CP4 solution, which is a mixture of 64% of nitric acid, 20% acetic acid  $\text{CH}_3\text{COOH}$  and 16% of fluorhydric acid to eliminate the impurities linked to the surface. The cleaned samples were treated by a mechanical polishing machine of model 920 working with different speeds combined with alumina abrasive in an alkaline solution and anodized during 25 min in a solution of diluted sulfuric acid with 66.66%  $\text{H}_2\text{SO}_4$  and 33, 33%  $\text{H}_2\text{O}_2$  at room temperature and with three different anodization currents (250 mA, 300 mA, 350mA). On the PA surface, c-Si was deposited by PECVD technique at 50 °C using a gas mixture of silane and  $\text{H}_2$  at a total pressure of 0.5 m Torr. The surface morphology of the films was examined by atomic force microscopy (AFM), which has been realized in plane-view for characterizing particles on wide areas. The determination of the pore diameter and statistics has been performed with the assistance of the SWxM program. The crystal quality of porous aluminium and the PECVD deposited c-Si was studied by means of XRD in  $\theta$ -2 $\theta$  configuration and confirmed by Raman spectroscopy.

The thermal properties such as the thermal conductivity and the thermal properties are determined by the PTD technique. This method whose principle is given in fig.1 consists in heating a sample with a modulated light beam of intensity  $I = I_0(1 + \cos \omega t)$  that will be absorbed on the surface and generates a thermal wave. This thermal wave will propagate in the sample and in the surrounding fluid (air in our case) and will induce a temperature gradient and then a refractive index gradient in the fluid. The fluid index gradient will cause the deflection  $y$  of a probe laser beam skimming the sample surface. This deflection may be related to the thermal properties of the sample. The sample is heated by a halogen lamp light of Power 100 W modulated by using a mechanical chopper at a variable frequency. An (He-Ne) laser beam skimming the sample surface at a distance  $x$  is deflected. This deflection can be detected by a four quadrant photodetector and converted to an electrical signal which is measured by a lock-in amplifier. Through the intermediary of interfaces, the mechanical chopper and the Look-in amplifier a microcomputer will set the desired modulation frequency and read the values of the amplitude and phase of the photo-thermal signal and then draw their variations according to the square root modulation frequency.

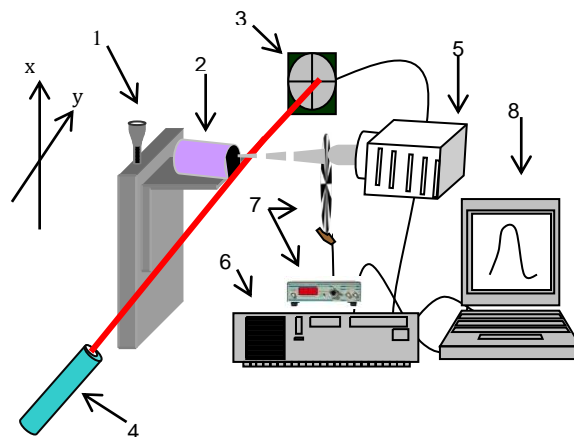


Fig. 1: Experimental set-up used for PTD investigation: 1-Table of micrometric displacement, 2-Sample, 3-Photodetector position, 4-Fixed laser source, 5-Halogen lamp, 6-Look-in amplifier, 7-Mechanical chopper, 8-Computer.

## 3. Results and discussions

### 3.1. Microstructural characterization

Fig. 2 shows AFM microscopy of these samples treated with three different anodization current intensities, in which is noted the presence of a quasi-arranged structure containing pores with width and

depth varying according to the current from 24 nm for  $I_a = 250\text{mA}$  to 73 nm for  $I_a = 350\text{mA}$ .

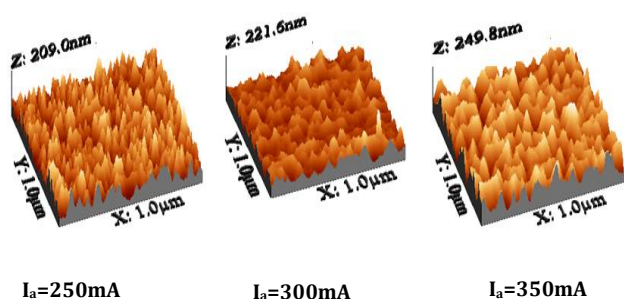


Fig 2: AFM images of Porous Aluminum (PA) layer versus anodization current intensity (250, 300, 350) mA.

These sizes are in good accordance with those obtained by Yan-fang Xu et al., 2015, when they demonstrate that the size vary with the anodizing potential from 53 nm to 130 nm. Fig. 3 shows the AFM microscopy analysis indicates that the nc-Si films deposited on these porous substrates present a nanogranular aspect with size estimated from the AFM scans from 50 to 85 nm as  $I_a$  increases.

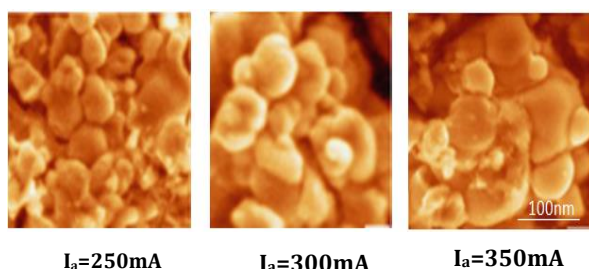


Fig. 3: AFM images of nanocrystalline silicon deposited on the porous aluminum for various anodization current intensity (250, 300, 350) mA.

Fig. 4 shows XRD spectra for the as deposited nc-Si thin layer. The deposited silicon seems to be crystallized and presented a preferred orientation in the (h01) direction.

Indeed, we notice two peaks indexed as the (101) and (201) direction. The two others peaks indexed as (200) and (220) are related to the aluminum substrate. The average crystallite size as deduced from the X-ray diffraction spectra using the Debye–Scherrer formula confirms the result mentioned above and increases as a function of  $I_a$  from 65 nm to 90 nm. These values are in accordance with the crystal size estimated from the AFM scans.

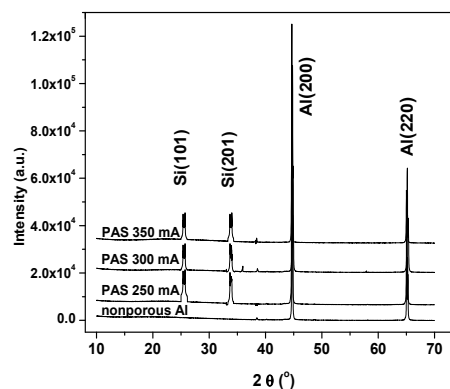


Fig. 4: XRD patterns of nanocrystalline silicon deposited on Porous Aluminum Layer versus the anodization current (250, 300, 350) mA .

In order to confirm the above mentioned results in term of crystallinity and sizes of grains, the Raman spectroscopy was performed which is reported in Fig. 5 for silicon films deposited directly on nonporous aluminum and porous one in which it shows an amorphous aspect, in fact the deposited films exhibit transverse optical band of crystalline Si located near  $526\text{ cm}^{-1}$  except for sample A1 which presents a peak at  $499\text{ cm}^{-1}$ .

The intensity of this peak increases and its position shift to high energies with the anodizing currents tending towards a peak corresponding to monocrystalline Si at  $528\text{ cm}^{-1}$ .

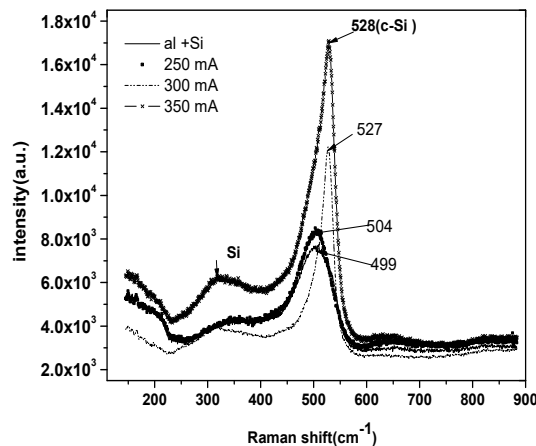


Fig. 5: Raman spectra of PASL prepared with different anodic current.

The crystallite size was calculated using the following formula.

$$\Delta w(D) = -A \left(\frac{a}{D}\right)^\gamma \quad (1)$$

Where  $D_w(D) = w_{C-Si} - w_{n-Si}$  and D are the Raman peak shift in nanocrystal as compared to monocrystalline silicon;  $a$  is the lattice constant of the silicon which is equal to 0.543 nm,  $A=47.41$  and  $\gamma=1.44$  are constants. The crystallite size estimated from this method was found between 75–110 nm when  $I_a$  varies from 250 to 350 mA respectively.

### 3.2. Thermal properties

The determination of thermal properties is made by the photo-thermal deflection technique, whose principle schema is shown in fig. 6, in which in the case of a uniform heating we have used a 1-dimensional approximation, and the amplitude and phase of the probe beam deflection is given by:

$$|\psi| = \frac{\sqrt{2}}{n} \frac{L}{\mu_f} \frac{dn}{dT_f} |T_0| e^{-\frac{x}{\mu_f}} \quad (2)$$

and

$$\varphi = -\frac{x}{\mu_f} + \theta + \frac{5\pi}{4} \quad (3)$$

Where L is the width of the pump beam in the direction of the probe laser beam, n,  $\mu_f$  and  $T_0$  are respectively the refractive index, the thermal diffusion length and the temperature of the fluid.

The quantities  $|\psi|$  and  $\theta$  are respectively the amplitude and phase of the temperature at the sample surface which are function of the thermal properties of the different media. The quantity x is the distance between the probe beam axe and the sample surface. Before the calculation of the probe beam deflection, it is essential to know the expression of the surface temperature  $T_0$  which is calculated as follow.

The sample is a stack of three layers; we write the heat equations in these three medias and in the surrounding fluid which is the air by designating  $K_i$ ,  $D_i$ , and  $l_i$ , respectively, the thermal conductivity, the thermal Diffusivity and the thickness of the layer i (1: aluminum, 2: porous aluminum filled or empty, 3: silicon or air)

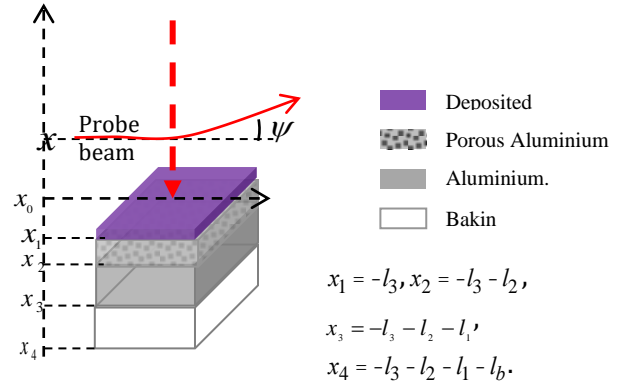


Fig. 6. The stacked three layers.

The resolution of the heat equation gives the following temperatures equations:

$$T_f(x, t) = T_0 e^{-\sigma_f x} e^{j\omega t} \quad \text{if } 0 \leq x \leq l_f \quad (4)$$

$$T_3(x, t) = (X_3 e^{\sigma_3 x} + Y_3 e^{-\sigma_3 x} - E_3 e^{\alpha_3 x}) e^{j\omega t} \quad \text{if } -l_3 \leq x \leq 0 \quad (5)$$

$$T_2(x, t) = (X_2 e^{\sigma_2(x+l_3)} + Y_2 e^{-\sigma_2(x+l_3)} - E_2 e^{\alpha_2(x+l_3)}) e^{j\omega t} \quad \text{if } -l_3 - l_2 \leq x \leq -l_2 \quad (6)$$

$$T_1(x, t) = (X_1 e^{\sigma_1(x+l_3+l_2)} + Y_1 e^{-\sigma_1(x+l_3+l_2)} - E_1 e^{\alpha_1(x+l_3+l_2)}) e^{j\omega t} \quad \text{if } -l_3 - l_2 - l_1 \leq x \leq -l_3 - l_2 \quad (7)$$

$$T_b(x, t) = W e^{\sigma_b(x+l_3+l_2+l_1)} e^{j\omega t} \quad \text{if } -l_3 - l_2 - l_1 - l_b \leq x \leq -l_3 - l_2 - l_1 \quad (8)$$

And after, we write the flow equation in each medium:

$$\phi_f(x, t) = K_f \sigma_f T_0 e^{-\sigma_f x} e^{j\omega t} \quad \text{if } 0 \leq x \leq l_f \quad (4p)$$

$$\phi_3(x, t) = -K_3 \sigma_3 (X_3 e^{\sigma_3 x} - Y_3 e^{-\sigma_3 x} - \frac{\alpha_3}{\sigma_3} E_3 e^{\alpha_3 x}) e^{j\omega t} \quad \text{if } -l_3 \leq x \leq 0 \quad (5p)$$

$$\phi_2(x, t) = -K_2 \sigma_2 (X_2 e^{\sigma_2(x+l_3)} - Y_2 e^{-\sigma_2(x+l_3)} - \frac{\alpha_2}{\sigma_2} E_2 e^{\alpha_2(x+l_3)}) e^{j\omega t} \quad \text{if } -l_3 - l_2 \leq x \leq -l_2 \quad (6p)$$

$$\phi_1(x, t) = -K_1 \sigma_1 (X_1 e^{\sigma_1(x+l_3+l_2)} - Y_1 e^{-\sigma_1(x+l_3+l_2)} - \frac{\alpha_1}{\sigma_1} E_1 e^{\alpha_1(x+l_3+l_2)}) e^{j\omega t} \quad \text{if } -l_3 - l_2 - l_1 \leq x \leq -l_3 - l_2 \quad (7p)$$

$$\phi_b(x, t) = -K_b \sigma_b W e^{\sigma_b(x+l_3+l_2+l_1)} e^{j\omega t} \quad \text{if } -l_3 - l_2 - l_1 - l_b \leq x \leq -l_3 - l_2 - l_1 \quad (8p)$$

The temperature and heat flow continuity at the interfaces  $x = -l_3, -l_3 - l_2$  permit to obtain:



To determine the changes of thermal properties of aluminum we start by determining the thermal properties such as the thermal conductivity  $K_2$  and thermal diffusivity  $D_2$  of the PA and we study the variation of the photo thermal signal for the same samples, which were filled by the silicon (PAS). The experimental variations of the amplitude and phase of photothermal signal are given respectively in Fig. 7 and 8.

To determine the thermal properties we have used the model with three layers (aluminum/(porous aluminum filled with silicon)/silicon) and we begin in a first step by introducing thermal properties of the deposited layer which are ( $K_3=0.15 W.K^{-1}.m^{-1}, D_3=0.38 \cdot 10^{-4} m^2.s^{-1}$ ) for the silicon nanocrystalline and ( $K_3=0.022 W.K^{-1}.m^{-1}, D_3=0.2 \cdot 10^{-4} m^2.s^{-1}$ ) for the empty porous aluminum and we introduce the thermal properties of the nonporous aluminum which are ( $K_1=273 W.K^{-1}.m^{-1}, D_1=0.94 \cdot 10^{-4} m^2.s^{-1}$ ) and in second step we compare the experimental signal with its corresponding theoretical, whereby the best fitting gives the values of the pair ( $K_2, D_2$ ).

After the simulation of the curves of figs. 7 and 8 the obtained values are given in Table 1 for the porous aluminum empty and filled with silicon, in which it is noted that they decrease with the anodization current for tending toward an average value of about  $131 W.m^{-1}.K^{-1}$  for both the porous aluminum empty or filled with silicon which characterizes the semiconductor material; for this, we can say that the introduction of thermal isolator material such as air or nc-Si in aluminum which is considered as a thermal conductor transforms it toward a thermal semiconductor.

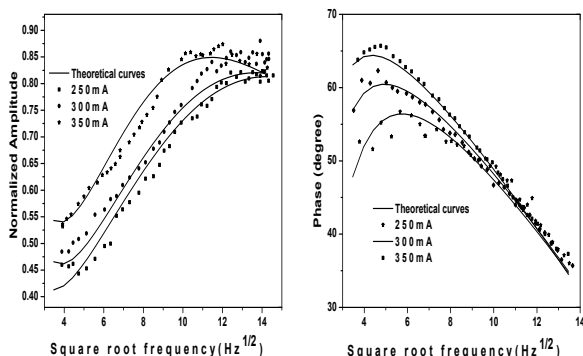


Fig. 7. Experimental and theoretical variation of the photothermal signal for the empty porous aluminum.

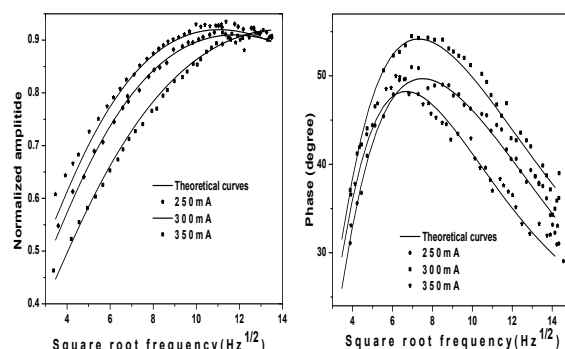


Fig. 8. Experimental and theoretical variation of the photothermal signal for the porous aluminum treated with different anodization current and filled with crystalline silicon.

Knowing the conductivity of porous layer can calculate the percentage of pores in the treated sample by using the Eq. 10, whose values are given in Table 1 where we remark its increase with anodizing current and has the same magnitude by using the PA or PAS values.

$$e = \frac{K_2 - K_1}{K_3 - K_1} \quad (10)$$

**Table 1:** Measured thermal properties, calculated porous density of the empty porous aluminum and porous aluminum filled with silicon and its gap energy for different anodization current intensities (250,300,350) mA.

	Empty Porous Aluminum			Porous aluminum filled with silicon		
	250mA	300mA	350mA	250mA	300mA	350mA
$\rho_p$	155.6±6	143±4	133±5	160±6	142±5	132±3
$D_2(cm^2.s^{-1})$	0.59±0.04	0.46±0.04	0.39±0.04	0.63±0.03	0.42±0.03	0.38±0.03
$\varepsilon(\%)$	43.1%	48.0%	52.1%	41.4%	48.0%	52.0%
$E_g(eV)$	-	-	-	2.03	2.01	1.99

### 3.3. Energy gap

Both the two materials PA and PAS are thermal semiconductors but only the PAS is an electrical semiconductor in which its energy gap is determined by using the Tauc method which implies that for energies  $E=h\nu$  higher than the energy gap  $E_g$ , the

quantity  $(\alpha E)^n$  varies with E according the relationship  $(\alpha E)^n = \beta(E - E_g)$  where  $\alpha$  is the absorption coefficient and b is the slope of the curve. For indirect band gap semiconductor such as nanocrystallineSi (nc-Si) deposited on porous

aluminum  $n = \frac{1}{2}$ . Then the curves of  $(\alpha E)^{1/2}$  versus  $E$  are shown in Fig. 9 on which it is indicated the linear part, whose intersection with the abscissa axis gives the energy gap.

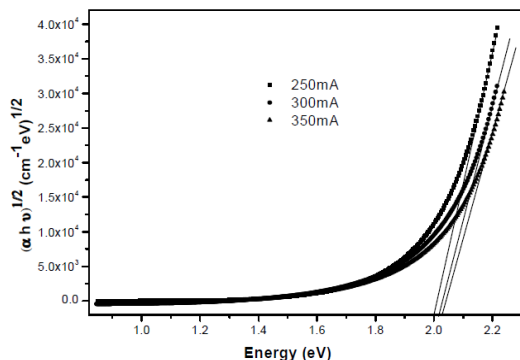


Fig. 9. Typical plot of  $(\alpha E)^{1/2}$  function versus photon energy  $h\nu$  with linear curves giving the PAS energy gap for various current intensities.

The obtained values are reported in Table 1 which shows that the energy gap decreases with the anodizing current from 2.03 to 1.99 eV marking a shift of about 40 meV; which has a more importance than that obtained for other works where we obtain a semiconductor with stable structure and middle gap energy whose its decrease can be attributed to the increase in porosity rate which is due to a decrease in the mean free path due to the phonon confinement in crystallite demonstrated and used by Lin et al., 2014 and Yao et al., 2015.

#### 4. Conclusion

Nano-crystallines silicon (nc-Si) whose sizes in 30–70 nm range were deposited by PECVD technique on porous aluminum (PA) layers which were prepared by the anodization technique for various current intensities. XRD, AFM and Raman measurements show that the pores are of cylindrical shape in the direction of the anodization current and presenting a diameter around 40 nm which increase with the anodization current intensity. Filling these pores with nc-Si transforms the aluminum material in its surface from a conductor to a semiconductor material whose energy gap is about 2eV has experienced a decrease of about 40 meV with increasing the porous density; and the thermal conductivity and diffusivity were determined by the photothermal deflection technique whose principle is described in detail which shows that they decrease with the porous density. This material has made the structural and physical properties that allow it to be

used in several energetic fields such as solar cells and heat exchangers.

#### Acknowledgements

This work was supported by the Scientific Research Deanship of University of Dammam, under Project no. 2014264.

#### References

- NielschK., ChoiJ., SchwirnK., WehrspohnR. B., and GoseleU., Nano. Lett. 2 (2002) 677-680.
- VrublevskyI., ParkounV., SchreckenbachJ., MarxG., Applied Surface Science 220 (2003) 51-59.
- GalcaA. C., KooijE. S., WormeesterH., and SalmC., Journal of applied physics 94 (2003) 4296-4305.
- TsengW. J.TsaiC. J., Journal of Materials Processing Technology, 146 (2004) 289-293.
- RamJ., SinghR., Applied Thermal Engineering 24 (2004) 2727–2735.
- KuA. Y., TaylorS. T., HewardW. J., DenaultL., LoureiroS. M., Microporous and Mesoporous Materials 88 (2006) 214-219.
- SamantrayP. K., KarthikeyanP., ReddyK.S., International Journal of Heat and Mass Transfer 49 (2006), 4209–4219.
- WangT. C., FanT. X., ZhangD., ZhangG. D., XiongD. S., Materials Letters 61 (2007) 1849–1854.
- AlinejadB., ZakeriM., Journal of Materials Processing Technology 209 (2009) 5042-5045.
- MurpheyM.B., BergesonJ.D., EtkornS.J., QuL., LiL., DaiL., EpsteinA.J., Synthetic Metals 160 (2010) 235-237.
- GhribM., GaidiM., KhedherN., GhribT., Ben SalemM., EzzaouiaH., Applied Surface Science 257 (2011) 3998-4003.
- LiuW., CanfieldN., Journal of Membrane Science 409–410 (2012) 113-126.
- SulkaG. D., BrzózkaA., LiuL., ElectrochimicaActa 56 (2011) 4972-4979.
- BarbosaE. F., SilvaL. P., Journal of Membrane Science 407–408 (2012), 128-135.
- WangX., LiC., ChenG., HeL., CaoH., ZhangB., Solid State Sciences 13 (2011) 280-284.
- HuangJ., RenH., SunP., GuC., SunY., LiuJ., Sensors and Actuators B: Chemical 188 (2013) 249-256.
- HuX., PuY.J., LingZ.Y., LiY., Optical Materials 32 (2009) 382-386.
- KurbanovS.S., Shaymardanov Z. S., KasymdzhanovM.A., KhabibullaevP.K., KangT.W., Optical Materials 29 (2007) 1177-1182.
- JuhászL., MizseiJ., Thin Solid Films 517 (2009) 6198-6201.
- Kashi M. A., RamazaniA., AbbasianH., KhayyatianA., Sensors and Actuators A: Physical 174 (2012) 69-74.
- WangT. C., FanT. X., ZhangD., Zhang G., XiongD. S., Materials Letters 61 (2007)1849-1854.
- KimK.P., LeeK.S., KimT.W., Woo D.H., Kim J.H., SeoJ.H., KimY.K., Thin Solid Films 516 (2008) 3633–3636.
- ZhuoH., PengF., LinL., QuY., LaiF., Thin Solid Films 519 (2011) 2308-2312.
- DygaR., WitezakS., Procedia Engineering 42 (2012)1088-1099.
- StojadinovicS., NedicZ., BelcaI., VasilicR., KasalicaB., PetkovicM., Zekovic L. j., Applied Surface Science 256 (2009) 763-767.
- BertolottiM., LiakhouG. L., FerrariA., RalchenkoV. G., SmolinaA., obrastsovaE., KorotoushenkoK. G., PimenovS. M., KonovV. I., J. Appl. Phys. 75 (1994) 7795-7798.

- GhribT., BejaouiF., HamdiA., YacoubiN., *ThermochimicaActa* 473 (2008) 86–91.
- GhribT., GaidI., YacoubiN., *Nondestructive Testing: Methods, Analyses and Applications*, eBooks, Nova publishers (2010) 95-146.
- Xu Y. F., Liu H., Li X. j., KangW. M., ChengB. W., LiX. J., *Materials Letters* 151 (2015) 79–81.
- LinY. C., ChaoY. T., YaoP.-C., *Appl. Surf. Sci.* 307 (2014) 724-730.
- YaoP. C., ChenC. Y., *Thin Solid Films* 579 (2015) 103–109.